Three-Dimensional Time-resolved Cardiovascular Magnetic Resonance Imaging based Particle Tracing: Recommendations

P.R. Roos

Technical Medicine | Imaging and intervention

November 2019 – July 2020

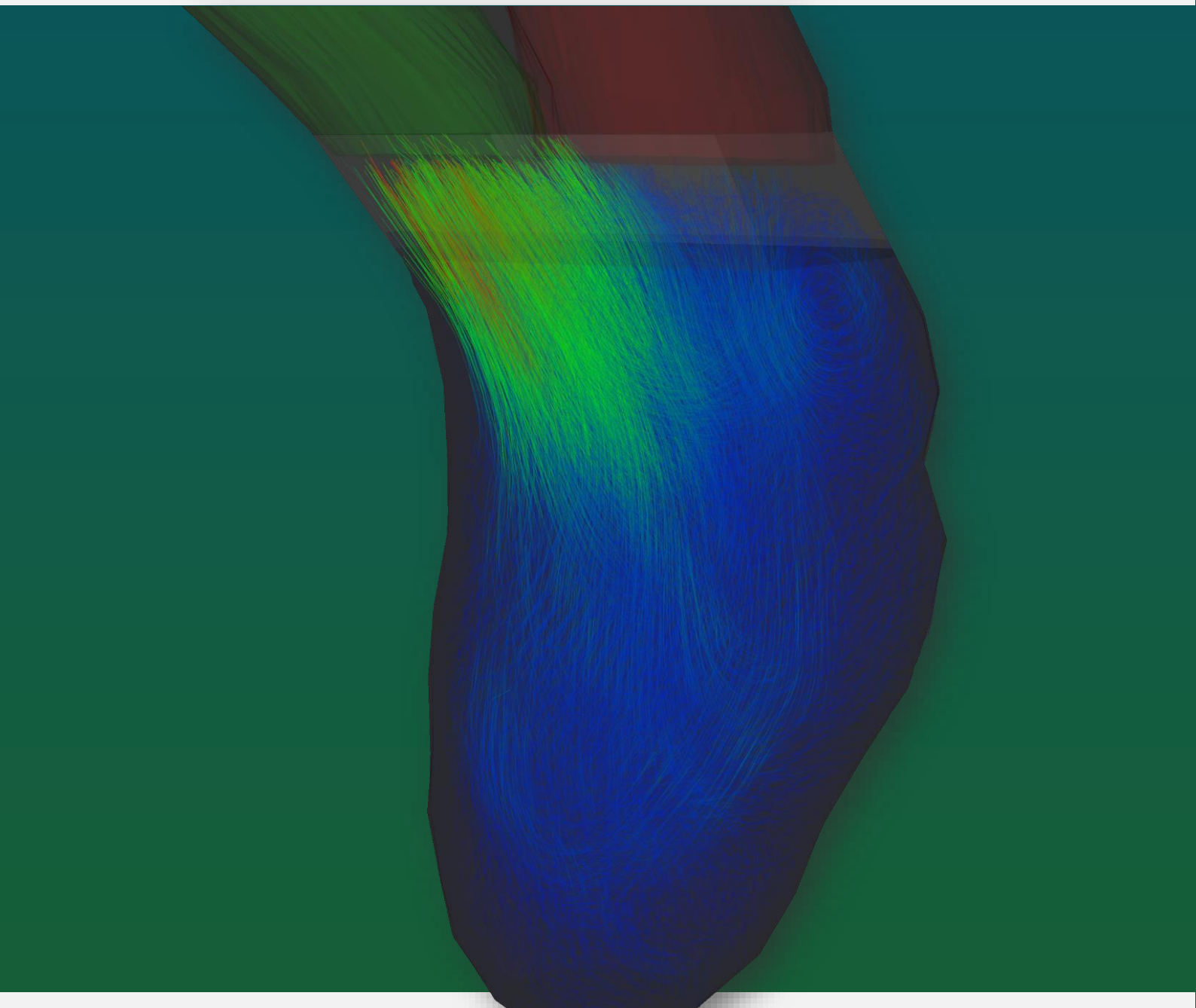

Universiteit Leiden

TU Delft Delft University of Technology

Erasmus Universiteit Rotterdam

THREE-DIMENSIONAL TIME-RESOLVED CARDIOVASCULAR MAGNETIC RESONANCE IMAGING BASED PARTICLE TRACING: RECOMMENDATIONS

- Effects of integration method, integration timestep and interpolation method on particle tracing outcomes -

Paul, Roos

Student number: 4375912

28 June 2020

Thesis in partial fulfilment of the requirements for the joint degree of Master of Science in

Technical Medicine

University Leiden; Delft University of Technology; Erasmus University Rotterdam

Master thesis project (TM30004; 35 ECTS)

Dept. of Biomechanical Engineering, TUDELFT

November 2019 – June 2020

Supervisor(s):

Dr. Ir. Jos J.M. Westenberg

Dr. Arno A.W. Roest

Dr. Ir. Hans C. van Assen

Thesis committee members:

Prof. dr. ir. Jaap Harlaar, *TU Delft (chair)*

Dr. Ir. Jos J.M. Westenberg, *LUMC*

Dr. Arno A.W. Roest, *LUMC*

Dr. Ir. Hans C. van Assen, *LUMC*

Dr. Dimitra Dodou, TU Delft, *Examination Board Technical Medicine*

Universiteit Leiden

TU Delft Delft University of Technology

Erasmus University Rotterdam

Abstract

Introduction

Cardiovascular magnetic resonance imaging (CMR) is an imaging modality from which the structure, function, perfusion, and metabolism of the cardiovascular system can be evaluated, which is essential in acquired and congenital cardiovascular disease (CVD). CMR can improve the outcomes of CVD during long term follow-up. 4D Flow MRI is a three-dimensional time-resolved CMR technique that uses phase contrast sequences with three-directional velocity-encoding and allows evaluation of the blood flow. 4D Flow MRI data can be analyzed with particle tracing.

Particle tracing is a technique that releases virtual particles in flow data (seeding) and traces the path the particles follow throughout the vasculature by integrating the flow data. The particle traces can subsequently be quantified with flow distribution analyses and visualized with pathlines, time-derived lines depicting the path particles have taken. Important settings for particle tracing are the integration method, integration timestep and data interpolation method. The aim of this research is to investigate the effect of different particle tracing settings on the accuracy and computation time and provide a recommendation on the use of particle tracing in 4D Flow MRI data and which particle tracing settings to aim for.

Methods

A particle tracing algorithm with a graphical user interface was developed for an existing inhouse developed 4D Flow post-processing workspace. Two 4D Flow MRI datasets from previous studies were acquired. One dataset was of a total cavopulmonary connection of a patient with Fontan circulation and the other was an intracardiac dataset of a healthy volunteer. Particle tracing with common settings and variations in integration method, integration timestep and data interpolation method was performed in both datasets and computation time, flow distributions (pulmonic distribution and four-component analysis), and number of particles that left the structure (missing particles fraction) and number of integration errors were quantified. The latter three were a measure of accuracy of the algorithm. Particle traces were subsequently visualized with pathlines.

Results

Particle with common settings gave a good accuracy for both datasets (missing particles fraction <20%). No differences in visualization, flow distributions and missing particles fraction were found for varying integration methods, interpolation methods and timesteps of 20ms or shorter. For timesteps of 30ms or longer, flow distributions changed compared to results with other settings and number of integration errors increased. Computation time increased almost linearly with the order of the integration method and almost inverted linearly proportional to the timestep. Retained inflow of four-component analysis was higher than normal values and direct flow was lower than normal values.

Discussion

For 4D Flow MRI based particle tracing we would recommend using a low order interpolator (e.g. a third

order Runge-Kutta integrator), a maximum timestep of half the temporal resolution of the data, and quadrilinear data interpolation. The results of the particle tracing tests with common settings were comparable to literature, except for the direct flow and retained inflow components of the four-component analysis. To enable accurate particle tracing, the particle seeding method must be chosen adequately and the MRI data and segmentations must be of good quality. Additional techniques such as segmentation shape interpolation and adaptive timestep control might be beneficial and their effect on the accuracy can be investigated in further research. As more advanced 4D Flow MRI acquisition techniques become available, their effect on particle tracing can be researched.

Contents

Introduction

Cardiovascular Disease

Approximately 18 million lives are lost every year due to cardiovascular disease (CVD), making it the leading cause of death worldwide.[1] Acquired CVD has an increasing prevalence, especially in people below 50 years of age, and congenital CVD is the most frequent congenital defect in live born.[2] Through advances in diagnosis, and pre-, peri- and post-operative care, the number of patients living with congenital CVD has increased dramatically, although important complications can reveal itself during long-term follow-up.[3] Nowadays, many CVDs can be predicted, prevented or treated. The most important factors for improving CVD outcomes are early detection, correct diagnosis, and adequate management of interventions during long term follow-up.

Acquired CVD includes coronary artery disease, coronary heart disease, rheumatic heart disease, diseases of the pulmonary vessels and the aorta, heart tissue disease and heart valve disease.[4] Acquired CVD can be asymptomatic and symptoms often only develop in advanced stages of the disease. Additionally, the symptoms are commonly non-specific such as shortness of breath, fatigue and oedema in extremities and the abdomen. There are only few specific (sub)clinical markers and as a result, acquired CVD is often underdiagnosed or diagnosed in a late stage of the disease.[5,6] A common type of acquired CVD is cardiomyopathy, dysfunction of the heart muscle tissue. Traditionally, cardiomyopathy is diagnosed by measuring the left ventricular ejection fraction, the fraction of left ventricular blood that is pumped in the aorta in one cardiac cycle, in combination with the patient's medical history and family history, but this can be inconclusive.[7]

Congenital CVD, or congenital heart defect, is the most common birth defect, with prevalence in about 49 million people globally in 2015.[8] The defects can cause a range of complications, from asymptomatic to life-threatening. If diagnosed and treated correctly, generally there is a good prognosis. However, congenital CVD are still the leading cause of birth defect-related deaths.[9] Treatment often consists of (open heart) surgery and lifelong specialized cardiac care, including regular follow-up examinations to assess the function of the cardiovascular system. Ventricular septal defect, atrial septal defects, and tetralogy of Fallot are the most common congenital CVDs, the latter being a combination of defects often seen together.[10] Defects in the heart valves are also common and can be asymptomatic, whereas transposition of the great arteries (TGA) is less common but life-threatening. Different surgical procedures have been developed to correct the defects or to palliatively improve the performance of the cardiovascular system. After correction or palliation of congenital CVD, significant morbidity is present during long-term follow-up, which necessitates regular imaging of the heart and great vessels.

4D Flow MRI

Cardiovascular magnetic resonance imaging (CMR or cardiovascular MRI) is an imaging modality from which the structure, function, perfusion, and metabolism of the cardiovascular system can be evaluated.

Each of these assessments can be performed without ionizing radiation, intravenous contrast materials or invasive procedures, making it very suitable for frequent follow-up.[11] 4D Flow MRI is a three-dimensional time-resolved CMR technique that uses phase contrast sequences with three-directional velocity-encoding. This technique allows for many different quantifications and visualizations of flow, such as flow volume and flow patterns, which is essential in cardiology.[12,13,14]

Phase contrast MRI is a technique in which phase signal is proportionally encoded to the velocity of moving spins.[15,16] This encoding is achieved by introducing bipolar gradients in the directions that are to be encoded. The measured phase can range from -180 degrees to 180 degrees. The velocity a measured phase corresponds to is determined by the user-defined encoding velocity (*venc*), where -180 degrees equals *-venc* and 180 degrees equals *venc*. This phase can be expressed in grey values which often range from black to

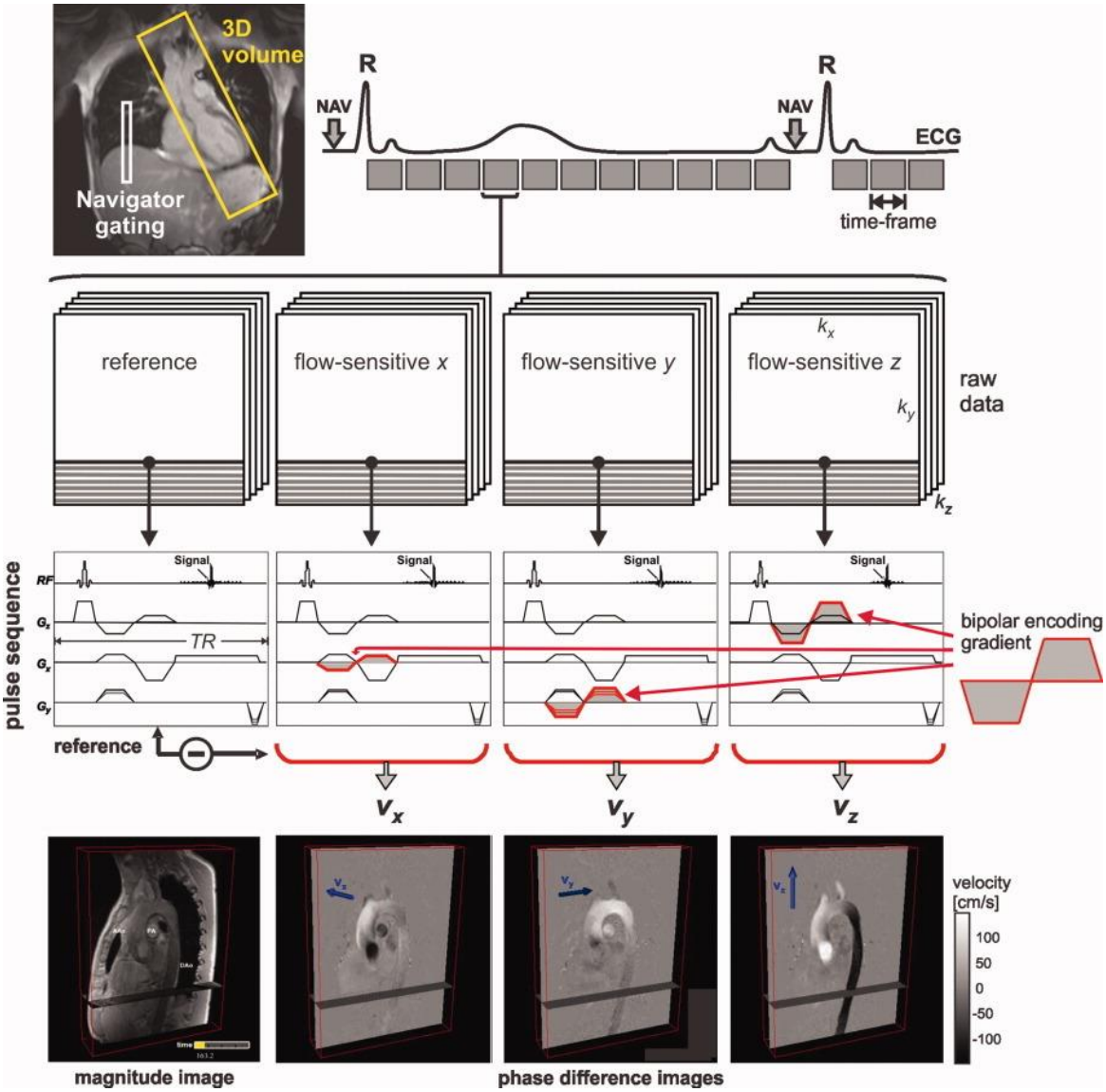

Figure 1: Schematic illustration of 4D Flow MRI of the thoracic aorta by Markl et al., 2012. For each time frame, four 3D datasets are collected: a reference scan and three velocity-encoded acquisitions in orthogonal directions. In this case, navigator gating of the diaphragm motion was used for image acquisition during free breathing.

white, where -180 degrees equals black, zero degrees equals grey and 180 degrees equals white. Velocities outside the range [-*venc*, *venc*] will cause aliasing, resulting in a mismatch of phase and velocity which causes artifacts in the data, as is the case when a *venc* is chosen too low. However, a higher *venc* also causes a low velocity to noise ratio (VNR) in areas with relatively low velocities.[17] The consensus is therefore to select a *venc* only slightly above the estimated maximum velocity.[18] The maximum velocity is estimated based on the average maximum velocities in the cardiovascular structure that is to be imaged. This estimation is not always possible, which is why using a robust and ideally error-free phase-unwrapping algorithm is recommended.[18] New acquisition techniques that use multiple *vencs* have been developed to prevent aliasing and increase VNRs.[19]

In 4D Flow MRI, a four-dimensional spatiotemporal volume scan is acquired over multiple cardiac cycles, from which at different timepoints in the cardiac cycle image volumes are reconstructed (see figure 1).[20] For regular velocity-encoding, at each of these timepoints (which are also called cardiac phases) four images are obtained: one reference image and three velocity-encoded images, one along each of three orthogonal directions.[16] After the acquisition, four time-resolved 4D datasets are generated: one magnitude dataset and three flow datasets representing velocities in each of the orthogonal directions. The temporal resolution and total scan time can be adjusted by the number of phases scanned.

Particle tracing

An important post-processing technique for 4D Flow MRI data is particle tracing. In this technique, virtual massless particles are released at chosen spatiotemporal locations and are traced as they traverse throughout the vasculature, under influence of the flow data.[21] This technique finds its origin in the analogue study of fluid dynamics and aerodynamics at the hands of researchers such as Leonardo Da Vinci.[22] By adding dyes or grain to water, Da Vinci was able to study the flow patterns that occur and similarly, by adding smoke to air, he was able to show flow patterns created by the wind.[23] Particle tracing is still mostly used in these areas of research, but now mainly in computational fluid dynamics and computational aerodynamics.[24,25]

In humans, 4D flow derived particle tracing can be used for visualization and quantification.[16,18] In so-called pathline visualization, the paths the particles follow are drawn to show the temporal evolution of the flow. These pathlines can be color-coded, e.g. to display the velocity. In quantification, the distribution of flow can be calculated by comparing the destinations of the particles. For example, this can be done in the left ventricle, where both the origin and destination of the particles can be used to categorize the particles and thereby assess the left ventricle function.[26]

Computational particle tracing

Unlike the analogue variant, digital or computational particle tracing requires algorithms to compute the path of the particle from the flow data. This calculation is done by integrating the flow data over time using iterative integration methods.[21] The simplest of these integration methods is the Euler Method, which is a first order integration method with a very limited accuracy. More popular for particle tracing are the Runge-Kutta methods, a family of higher order iterative integration methods. The higher order methods are more

precise, but more computationally expensive. As a compromise between computation time and accuracy, the fifth order Runge-Kutta method (RK45) is often chosen.[26,27]

Besides the integration method itself, the accuracy of iterative integration depends on the time interval that is integrated over, also called the timestep. When applied to ordinary differential equations, a longer timestep means less accurate approximate solutions at the benefit of less steps to be calculate for the same time interval. The opposite is also true: a shorter timestep results in more accurate solutions at the cost of more steps to be calculated for the same time interval. Flow data cannot be properly described with ordinary differential equations, so a shorter timestep does not necessarily mean an increase in accuracy.

4D Flow MRI scans are discrete in both space and time, due to a sampling process during acquisition, but the virtual particles in particle tracing can exist between these discrete spatiotemporal points. Therefore, interpolation is used to construct new data points in between the data points of the flow data. The data is often interpolated linearly in the temporal dimension, whereas the signal in the three spatial dimension is often interpolated using linear, cubic or advances splines interpolation. The choice for the interpolation method can have a large impact on computation time due to the multidimensional aspect of the data.[28] For example, in a single dimension, the cubic interpolation method averages two times as many points as the linear interpolation method (4 points vs. 2 points for cubic and linear interpolation, respectively). In four dimensions, this would mean that the cubic interpolation averages 16 times as many points (4^4=256 vs. 2^4=16 points in total for cubic and linear interpolation, respectively), which requires more calculation steps. More advanced interpolation creates better and smoother visualizations, but the quantitative effect of the interpolation method on the accuracy of particle tracing in medical data has not been described yet.[28]

The accuracy of particle tracing can be measured in different ways, depending on the application of particle tracing.[27,29,30] In all cases, the number of particles that leave the cardiovascular structure through the vascular wall, also called missing particles, can be measured. The ratio between the missing particles and the total amount of particles seeded can be used as a measurement of accuracy and Ha et al. have suggested using this ratio as a cut-off condition.[30] For left ventricle particle tracing, the ejection fraction calculated from particle traces can compared to the ejection fraction that has been measured with an echocardiogram.

Study aims

4D Flow MRI based Particle tracing can be a unique tool to visualize and quantify blood flow in cardiovascular structures, but there is no clear advice as to which settings, such as interpolation method, integration method, and timestep length, should be used to perform the analysis accurately and quickly. In other research areas such as computational fluid dynamics, recommendations on using particle tracing have been given, but not for particle tracing in medical data. In this study, we aim to investigate the effect of different particle tracing settings on the accuracy and computation time and provide a recommendation on the use of particle tracing in 4D Flow MRI data and which particle tracing settings to aim for.

Methods

Pythonviewer

Many commercial post-processing software packages have been developed for 4D Flow MRI data, of which many can perform particle tracing. However, these packages do not allow changing most of the settings which are necessary for this research, such as the timestep and integrator type. Particle tracing was therefore implemented in the Pythonviewer (figure 2), a post-processing workspace developed within the Cardiovascular Imaging Group (CVIG) of the Leiden University Medical Center. This workspace allows visualization and quantification of cardiovascular imaging data and has been built for research purposes. It can handle medical images saved in the common DICOM format and uses the Python Imaging Library (PIL) and wxPython packages to display the data. The Visualization Toolkit (VTK), which is developed by Kitware, is used for additional visualization and quantification options.[31] For data representation and numerical computations, the Python package NumPy was used.[32] Particle tracing was not yet implemented in the Pythonviewer and, therefore, a particle tracing algorithm and an application-specific graphical user interface (GUI) were therefore developed for this research.

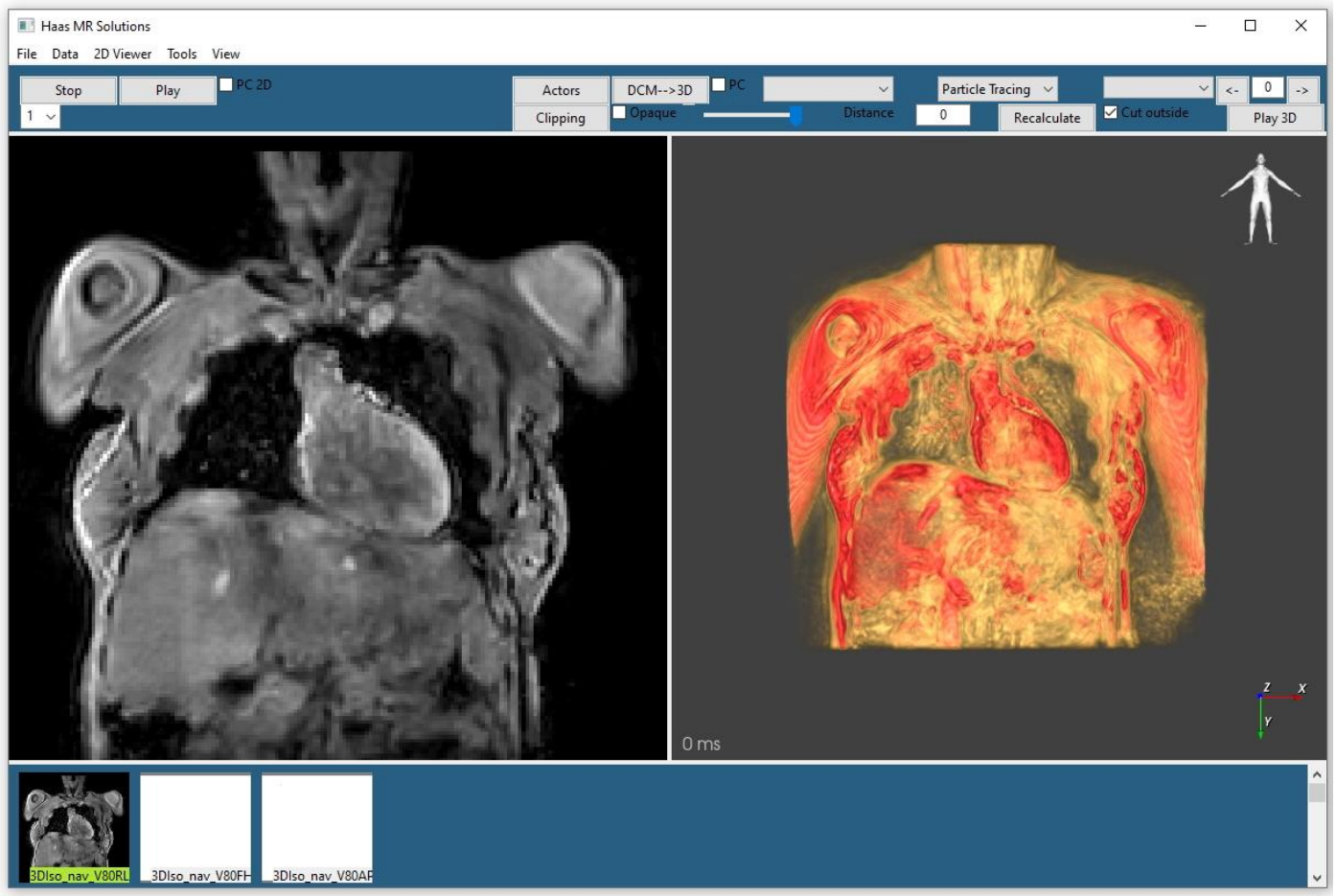

Figure 2: The PythonViewer interface with a 4D Flow MRI scan loaded and visualized. The left viewport shows a magnitude image of the scan in standard grayscale slice visualization, whereas the right viewport displays a 3D volume rendering of the magnitude image.

Particle tracing algorithm

The implemented particle tracing code consists of three parts: the GUI, the particle tracing algorithm, and the visualization algorithm. The GUI (figure 3) can be used to initiate the particle tracing, change the algorithm's settings, and export the calculated particle traces. It is divided in three sections: the top section contains the main controls to save and delete particle traces, initiate the particle tracing and to initiate or delete the visualization. The middle section contains the main settings of the particle tracing: the seeding method, the seeding time, the integration method, the initial and maximum timestep, and the interpolation method. The bottom section contains the settings for the seeding grids, which are used in case instantaneous seeding method is chosen.

The particle tracing algorithm itself consists of five parts, as can be seen in the flowchart in figure 4. The first part is the seeding, in which it determines at what spatiotemporal location particles are placed, which depends on the chosen seeding method. For instantaneous seeding, the particles are placed on the grid points of a user-defined seeding grid at the user-defined seeding time. If a structural mesh, such as a segmentation of the vasculature, is loaded, the algorithm excludes any particles that are outside of this mesh. This is useful for when the rectangular seeding grid fills a cross-section of the vasculature, but the corners exceed the vasculatures boundaries. For intracardiac seeding, particles are placed in the centers of the voxels that are within the predefined left ventricle segmentation. An inward margin of approximately the size of one voxel is taken for the left ventricle segmentation to avoid seeding too close to the myocardial wall. Seeding the particles, allocating system memory, and loading user-defined settings are together seen as the initialization.

The second part of the particle tracing is the integration. Per particle, the flow data of its current spatiotemporal position is integrated over a timestep to calculate the particles new spatiotemporal position. This is done using the SciPy library, a toolkit for Python with configurable integrator methods.[33] This toolkit has multiple integrator functions, including higher order integrators. For every particle, an integrator is setup and the integrator takes steps. For every step, the time, spatial coordinates, and velocity of the particle is recorded.

The third part of the algorithm is the function which interpolates the data that the integrator calls upon. The linear interpolation has been written as a Python script, whereas the tricubic interpolation method uses the 'pytricubic' module which has been created by Daniel Guterding and utilizes a C++ library. This tricubic interpolation is based on the tricubic interpolation algorithm by Lekien and Marsden.[34] This algorithm is based on a specific 64 × 64 matrix that gives the relationship between the derivatives at the corners of elements and the coefficients of the tricubic interpolant for these elements. For tricubic interpolation, this matrix is initialized per cardiac phase before integration starts, which can increase computing time before integration and decrease computing time during integration. Interpolation over the time dimension was linear in both integration methods.

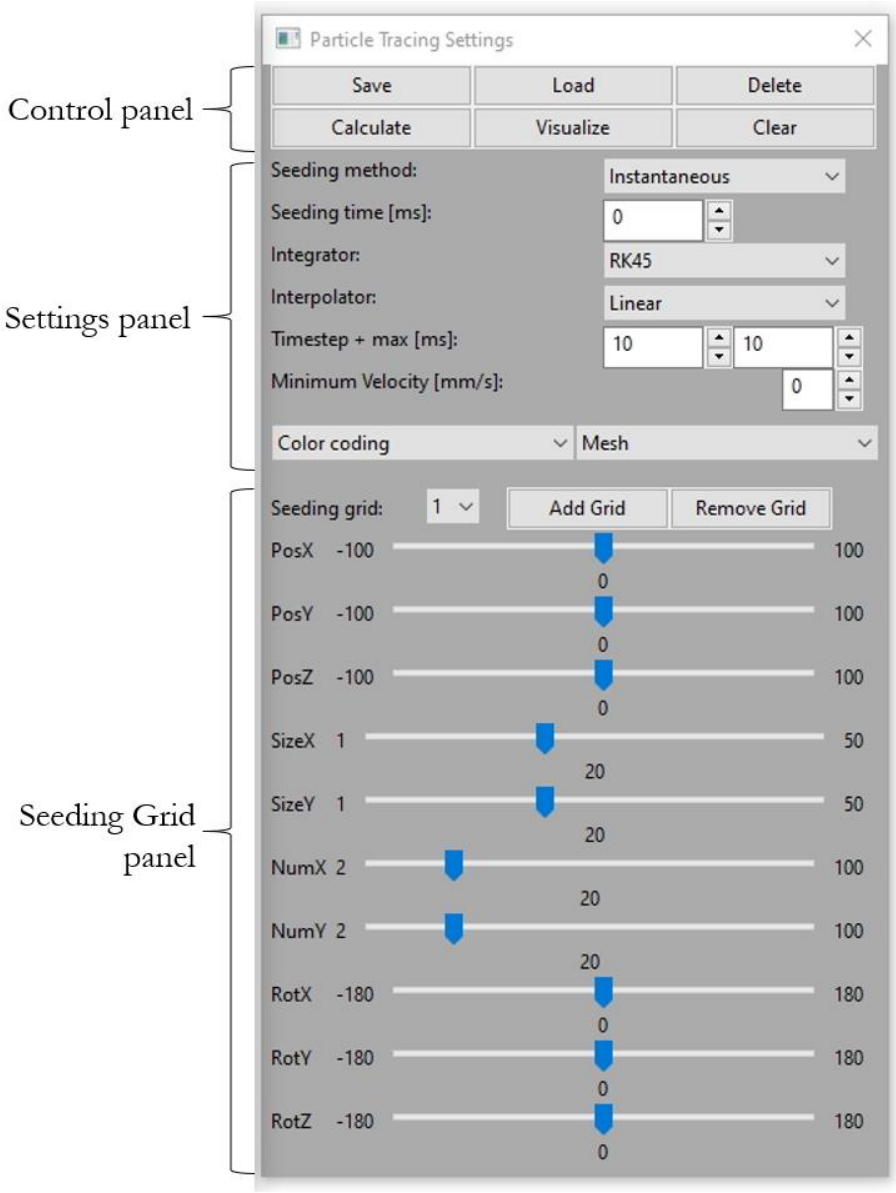

Figure 3: Particle tracing graphical user interface (GUI). This interface was developed for this research and allows choosing particle tracing settings.

The fourth part of the particle tracing algorithm is the reporting of quantitative particle tracing results. This part displays the results of the accuracy measurements and the additional measurements, such as the computation time. Virtual counters are used whenever a particle's tracing stops, to categorize the particle by its destination, such as a specific cardiovascular structure. These counters are then used to create the measurements results.

The particles are traced until a stopping condition is met. This can be that the location of the particle is inside or outside a specific cardiovascular structure, that the particle moves slower than a user-defined threshold, or that a user-defined integration limit such as a maximum number of integration steps is reached. In this research, neither velocity nor the amount of integration steps were used as a stopping condition, but only the location of the particle with respect to segmentation models, as described further on.

The fifth part is the visualization of calculated particle traces, which is programmed to be performed in one of two ways: all at once or in cine mode. When drawn all at once, the entire paths each particle takes are drawn. This static visualization does not show the temporal aspect of the pathlines (unless temporal color coding is used) and is mainly used for a visual inspection of the algorithm's performance. For the cine mode visualization, a frame is drawn for a time interval containing the pathlines that are within that time interval

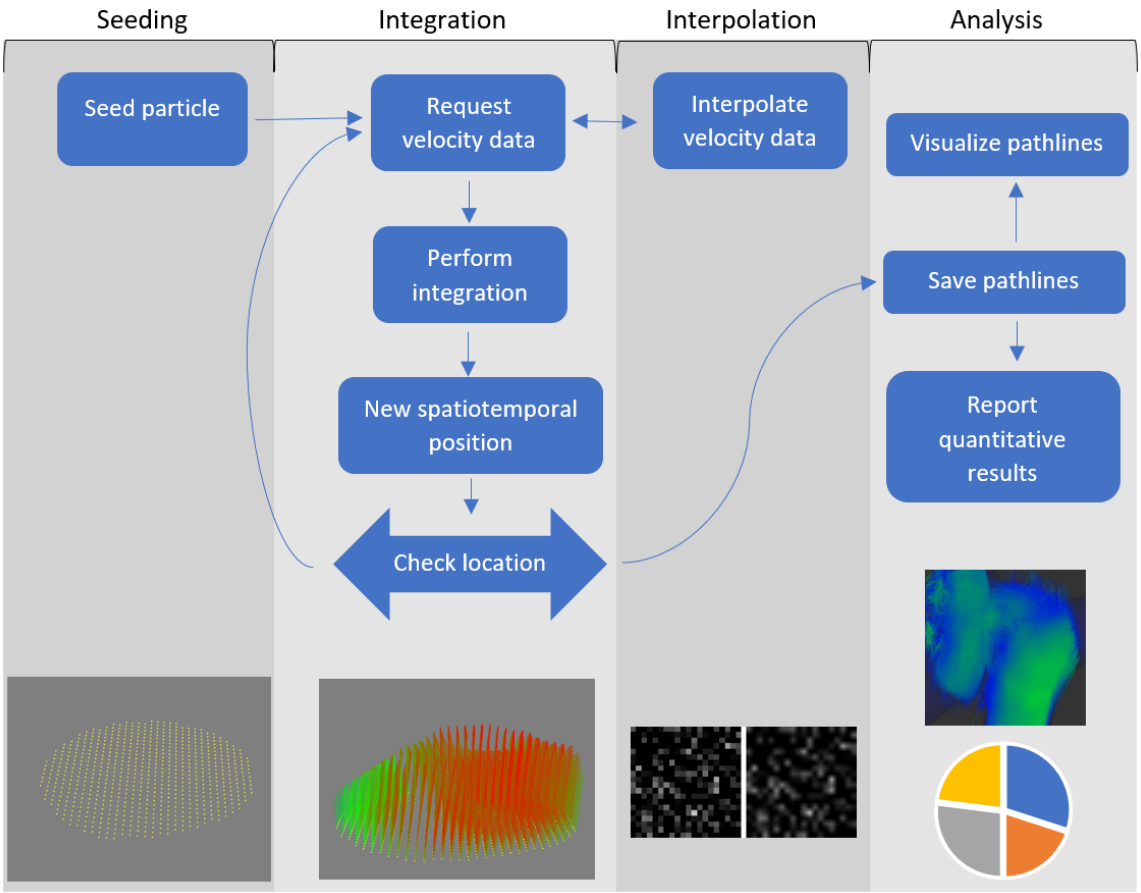

Figure 4: Flow chart describing the particle tracing algorithm. The integration section is performed for every particle and the interpolation is performed for every integration step.

or in adjacent time intervals, also called streamlets. This is done for every time interval that pathlines exist in. These frames are then combined into an animation by ordering them by time. This dynamic visualization of pathlines is used in clinical practice to investigate the flow patterns. Color-coding can be used to give additional information to the particle traces. A commonly used color-coding is velocity color-coding, where the velocity of the pathline segment is visualized with a corresponding color. The color-coding used for the pathlines in this research is a relative velocity color-coding with colors ranging from blue to green to red, whereas pure blue is a velocity of zero and red is the maximum velocity a segment in the particle tracing data has.

Experiment methods

Particle tracing with different settings was performed on two different 4D Flow MRI datasets. One dataset is of a patient with a total cavopulmonary connection (TCPC) resulting from a Fontan procedure. This scan was performed for the VELOCITY study, a study by the LUMC and the University Medical Center Utrecht.[35] The other 4D Flow MRI dataset is a scan of the heart of a healthy volunteer. This scan was performed for a previous study on flow patterns in patients with a corrected atrioventricular septal defect (AVSD).[36] The datasets will be called the *Fontan dataset* and the *Intracardiac dataset,* respectively. Both studies were reviewed and approved by the Medical Ethical Committee and the patient and volunteer both had provided written informed consent.

The aim of the experiment is to measure the effect of different settings on the computation time and accuracy of particle tracing. The different settings that were used were the interpolation method, the integration method and the timestep. For the interpolation method, the options used were four-dimensional linear (quadrilinear) interpolation and three-dimensional cubic (tricubic) spatial interpolation with linear interpolation in the dimension of time.[34]

There were three options for the integration method: third order Runge-Kutta, fifth order Runge-Kutta and eighth order Runge-Kutta. These integration methods were based on the SciPy library functions RK23, RK45 and DOP853, respectively.[33] It is worth noting that these integration methods were based on the Runge-Kutta families as described by Dormand and Prince and not the integration methods described by other researchers, such as Fehlberg.[37,38] Each integration method has a built-in adaptive timestep control that repeats an integration step with a smaller timestep if the estimated error of the integration step exceeds a user-defined tolerance. The timestep is also increased for the next integration step if the estimated error is deemed small enough, until the maximum timestep is reached. The mentioned error estimation is performed by comparing the integration step results with a result of a lower order integration method. While this adaptive timestep control can be useful in actual practice, it is not used in this research to study the effects of the timestep on the accuracy and calculation time of the particle tracing algorithm.

The timesteps that were used in this research were 1ms, 5ms, 10ms, 15ms, 20ms, 30ms, 50ms, 75ms and 100ms. The total number of particle tracing tests that were performed were therefore 24, of which 12 per dataset. The different settings per test are given in table 1. Given the most used settings for particle tracing in current literature, test #1 and test #13 are considered the standard settings with a quadrilinear interpolation method, a fifth order Runge-Kutta integration and a timestep of 10ms. The settings of the other tests will therefore mostly vary from these standard settings in only a single variable. The total computation time was measured from the moment the algorithm started and until the last particle was traced. The time it took to seed the particles, allocate system memory, and load user-defined settings was measured as initialization time. The time of the particle tracing itself, excluding the algorithms setup and reporting steps, was also measured. Particle tracing is considered to be inaccurate if many particles leave the vasculature; given that the particles represent volumes of blood, blood should not leave the vasculature unless the patient was bleeding internally. Therefore, the accuracy was measured by measuring the lost particles fraction for both data sets. Particles were considered part of the lost fraction if they were more

Table 1: The settings used in the particle tracing tests

Test #	Dataset	Interpolator	Integrator	Timestep [ms]
1	Fontan	Quadrilinear	RK45	10
2	Fontan	Tricubic	RK45	10
3	Fontan	Quadrilinear	RK23	10
4	Fontan	Quadrilinear	DOP853	10
5	Fontan	Quadrilinear	RK45	1
6	Fontan	Quadrilinear	RK45	5
7	Fontan	Quadrilinear	RK45	15
8	Fontan	Quadrilinear	RK45	20
9	Fontan	Quadrilinear	RK45	30
10	Fontan	Quadrilinear	RK45	50
11	Fontan	Quadrilinear	RK45	75
12	Fontan	Quadrilinear	RK45	100
13	Intracardiac	Quadrilinear	RK45	10
14	Intracardiac	Tricubic	RK45	10
15	Intracardiac	Quadrilinear	RK23	10
16	Intracardiac	Quadrilinear	DOP853	10
17	Intracardiac	Quadrilinear	RK45	1
18	Intracardiac	Quadrilinear	RK45	5
19	Intracardiac	Quadrilinear	RK45	15
20	Intracardiac	Quadrilinear	RK45	20
21	Intracardiac	Quadrilinear	RK45	30
22	Intracardiac	Quadrilinear	RK45	50
23	Intracardiac	Quadrilinear	RK45	75
24	Intracardiac	Quadrilinear	RK45	100

RK45 = Fifth order Runge-Kutta integration; RK23 = third order Runge-Kutta integration; ODE853 = eighth order Runge-Kutta integration.

than 5 mm outside of the segmentation models. This 5 mm margin, approximately the length of two voxels, was chosen to compensate for segmentation inaccuracies. For the intracardiac dataset, a four-component analysis, as proposed by Eriksson et al. and described further on, was also performed.[26] For the Fontan dataset, the distribution of flow from the superior and inferior vena cava (SVC and IVC, respectively) to the left and right pulmonary artery (LPA and RPA, respectively), was also measured.[30,39]

The SciPy integration methods have a built-in function to test whether the integration can be performed accurately with the given timestep. This can give errors if the size of the calculated step is too little, which happens if the particle leaves the boundaries of the 4D Flow data. This is possible with timesteps that are too long, as the particle can move too close to the boundaries of the data, resulting in errors in the next step. Additionally, integration errors can occur if the integration method cannot accurately calculate a step due to other reasons, such as a too large timestep. If integration errors occur, particle tracing is terminated for the particle that was being traced. The amount of errors was recorded and particles the tracing of which gave errors were excluded from further analysis.

The tests were performed on a computer with an AMD 2600x hexacore processor running at 3.7GHz and 16GB of RAM running at 2933MHz. No multi-core optimizations or GPGPU (General-purpose computing on graphics processing units) were performed and thus the algorithm only ran on a single CPU core. As most software packages have these optimizations, the results of the computing time measurements should not be taken as a real-world example of clinical use.

Fontan data

The 4D Flow MRI scan from a patient with a total cavopulmonary connection (TCPC) was performed on a Philips Ingenia MRI scanner with a magnetic field strength of three Tesla (3T). The scan consists of 24 phases of 27 slices, with 176 by 176 voxels per slice. The voxels are isovolumetric with a length of 2.08mm. A Venc of 80cm/s was chosen and the temporal resolution (time between phases) was around 37ms. The data was made cyclic by repeating the cardiac phases in order in the interpolation algorithm. A segmentation of the TCPC was created by an experienced physician. Virtual cubes were placed at the connection of the left and right pulmonary artery with the TCPC, as can be seen in figure 5 (LPA-C and RPA-C). An additional cube was placed on a superior branch of the right pulmonary artery, as this branch was connected to the TCPC itself as well (RPAB-C).

Seeding was performed using a continuous seeding method: particles were released from grid points of two seeding grids at every timeframe of the 4D Flow data. The two seeding grids were placed in the inferior vena cava and superior vena cava, perpendicular to the vessel. Due to the larger diameter of the inferior vena cava, the inferiorly placed seeding grid contained 40 by 40 (1600) grid points while the superiorly placed seeding grid contained 30 by 30 (900) grid points. Grid points that were outside of the 3D segmentation model or within one voxel-length of the segmentation's wall were automatically excluded and no particles were released from these grid points. Particle tracing itself was performed over the course of two cardiac cycles.

The distribution of pulmonic flow, henceforth called pulmonic distribution (PD), was calculated from the particles' origins and destinations: The percentage of particles that enter the LPA or RPA (or go missing) was reported for particles seeded from both the SVC and IVC individually. The ratio of particles that reached the LPA and RPA, and the ratio of particles that went missing was also reported. If particles were still in the TCPC structure at the end of the second cardiac cycle, they were reported as part of the remaining fraction. This fraction is ideally low, as this would mean that particle tracing was not stopped prematurely. As mentioned before, particles the tracing of which gave an integration error were recorded and excluded from further analysis, such as the PD analysis.

Intracardiac data

The 4D Flow MRI scan from a healthy volunteer for the beforementioned AVSD study was also performed on a Philips Ingenia 3T MRI scanner. This scan consists of 30 phases of 39 slices, with 176 by 176 voxels per slice. The voxels have a length and width of 2.27mm with a slice thickness of 3.00mm. A Venc of 150cm/s was chosen and the temporal resolution was around 28ms. The data was made cyclic by repeating the cardiac phases in order in the interpolation algorithm. Segmentations of the left ventricle, aorta and left atrium were created for every phase and slice by an experienced physician using manual segmentation tools of inhouse developed Cardiac MRI analysis software. 3D models were created from the segmentations, as can be seen in figure 6. The models of the aorta and left atrium were not connected to the left ventricle model, because of the conversion of a slice-based segmentation to a 3D model. A cuboid model encompassing at least the aortic valve, the mitral valve and the parts of the other 3D models that were closest to these valves, was created for every phase (CON in figure 6). Particles that had left the left ventricle

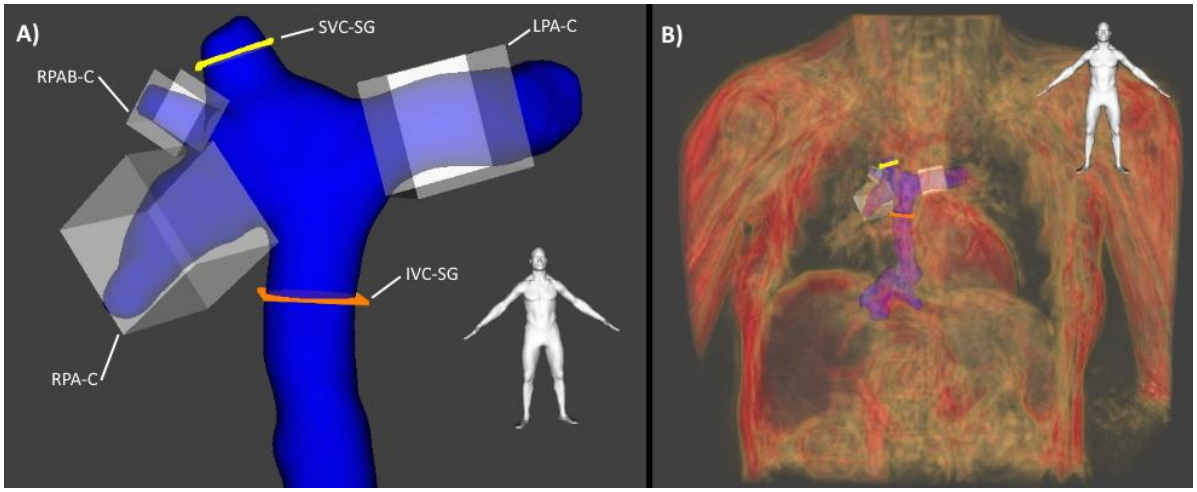

Figure 5: 3D models of the TCPC and counter cubes of the Fontan dataset with seeding grid (A) without MRI data and (B) with MRI magnitude data rendered using volume rendering. Both images are in anterior-posterior orientation and a 3D human anatomical model is drawn to visualise patient orientation. *TCPC = Total Cavopulmonary Connection; SVC-SG = Superior Vena Cava seeding grid; IVC-SG = Inferior Vena Cava seeding grid; LPA-C = Left Pulmonary Artery counter cube; RPA-C = Right Pulmonary Artery counter cube; RPAB-C = Right Pulmonary Artery branch counter cube*

model and were not in the left atrium or aorta model, were considered part of the missing particles fraction, unless they were still in the connection model. The location of the particle in relation to the segmentation models was done by selecting the segmentation models of the cardiac phase that the particle was temporally closest to, a so-called nearest-neighbor approach.

Seeding was performed using an instantaneous intracardiac seeding method: particles were released from each voxel within the LV segmentation model at the time of isovolumetric contraction (end-diastole). This is the moment within the cardiac cycle where the left ventricle is at its largest and both the aortic and mitral valves are closed, so no blood enters or leaves the left ventricle. Voxels within a voxel-length of the left ventricle wall were excluded and no particles were released from these voxels. Particle tracing was performed over the course of one cardiac cycle. Particles were traced forwards in time until the moment of isovolumetric relaxation (end-systole), where both the aortic valve and mitral valve are closed again. Particles were also traced backwards in time until the moment of isovolumetric relaxation as well. Figure 7 is a Wiggers diagram that shows the ventricular volume in relation to the echocardiogram signal.[40] In the intracardiac data, the point of isovolumetric relaxation was determined to be the timeframe with the smallest LV volume and the point of isovolumetric contraction was determined to be the timeframe with the largest LV volume. As can be seen in figure 7, the LV volume can be constant from mid-atrial systole on or even larger in atrial systole than in isovolumetric contraction, but this was not the case for the used dataset.

A four-component analysis was performed by categorizing the particles in four categories based on their origin and destination, as described by Eriksson et al (figure 8).[26] The categories *Direct Flow* and *Retained*

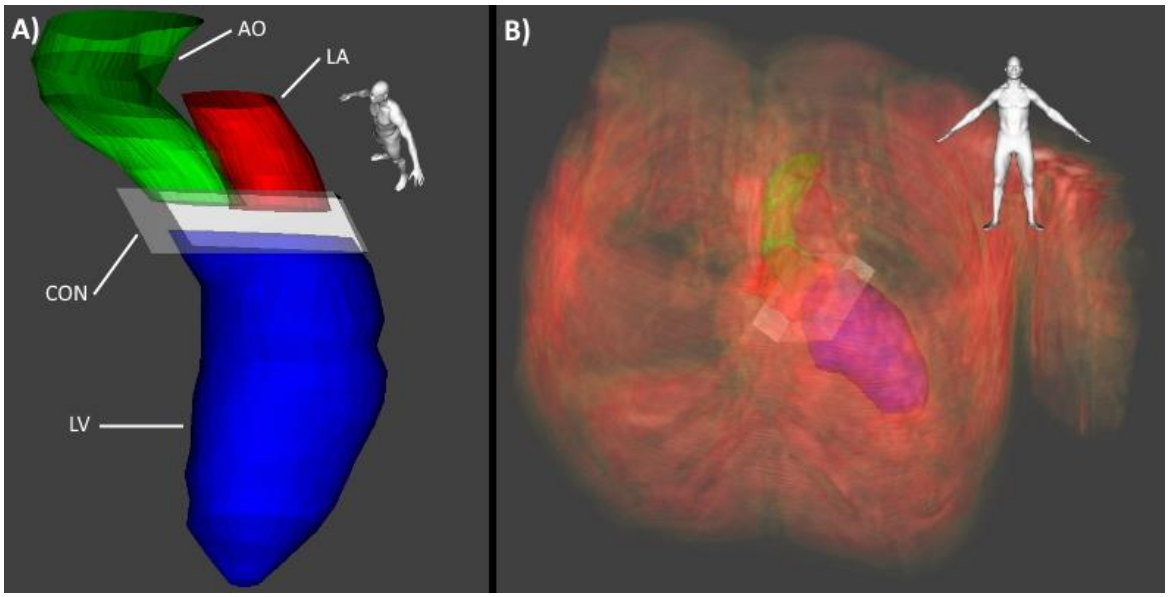

Figure 6: 3D models of the Left Ventricle (LV), Aorta (AO), Left Atrium (LA) and a connection cuboid (CON) (A) without MRI data and (B) with MRI magnitude data rendered using volume rendering. Figure 3A is in an oblique superior-inferior orientation and figure 6B is in an anterior-posterior orientation. A 3D human anatomical model is drawn to visualise patient orientation.

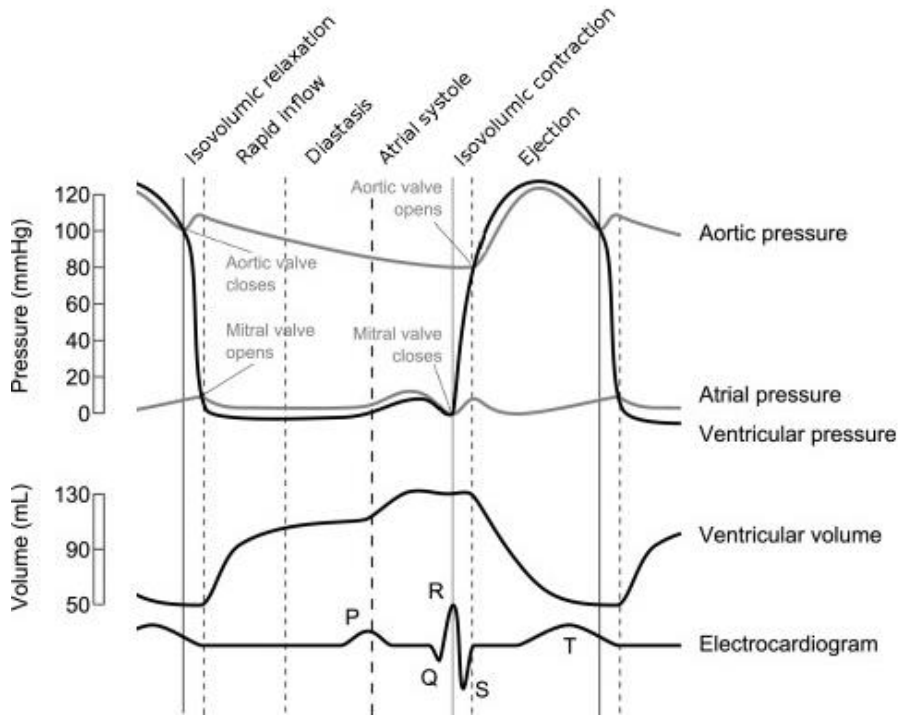

Figure 7: Wiggers diagram. The figure shows the aortic, atrial, and ventricular pressure and the ventricular volume in relation to the electrocardiogram signal. The ventricular volume is lowest at the point of isovolumic relaxation and highest at the point of isovolumic contraction.

Inflow contained particles that during a single cardiac cycle entered the LV through the mitral valve and respectively left through the aortic valve or remained in the LV. The category *Delayed Ejection Flow* contained particles that during a single cardiac cycle were already in the LV and left through the aorta. The category *Residual Volume* contained particles that were already in the LV and stayed in the LV during a single cardiac cycle. Particles that left the LV through other means, either in systole, diastole, or both, were excluded from the four-component analysis and were noted as part of the lost fraction. Particles whose tracing gave an integration error were recorded and were not part of further analysis, such as the four-component analysis.

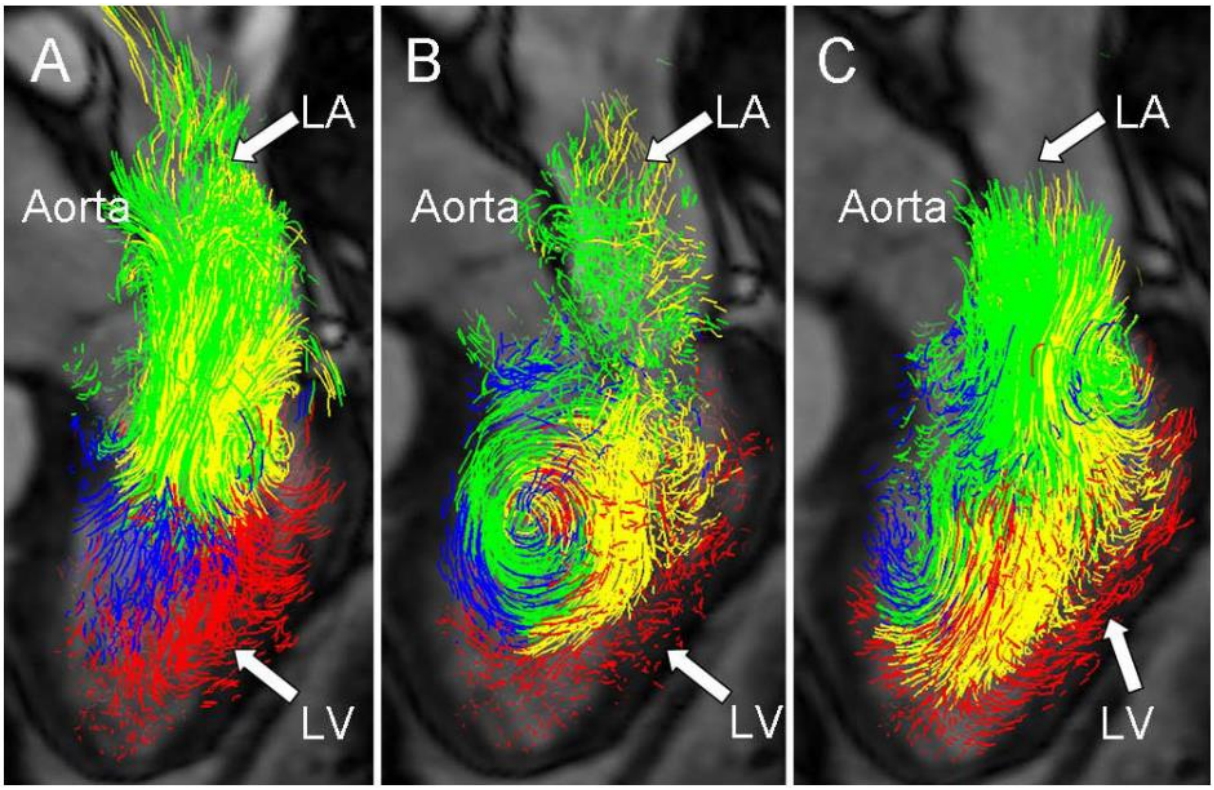

Figure 8: Pathline visualization of all blood flow involved in one cardiac cycle in the left ventricle in a healthy patient. The four-component color coding of Eriksson et al. is applied. A: Early LV filling; B: Diastasis; C: Atrial contraction.

Results

Fontan dataset

The results of the 12 particle tracing tests that were performed on the Fontan dataset are noted in Table 2. Test 1 is considered the standard settings and other tests only vary in a single variable to this standard test. The interpolation method is only different for test 2, whereas the integration method varies for tests 3 and 4. The other tests, 5 to 12, have different timesteps.

Interpolation method

In the comparison of test 1 and test 2, differences in both pulmonic distribution and missing fraction are under one percent of the total of the particles seeded. Only the missing fraction of particles seeded from the SVC is more than one percent higher for the tricubic interpolation method (1.28%), which is due to a lower fraction of particles that had the same origin but a different destination. Total computation time and particle tracing time for the tricubic interpolation method was less than half of the linear interpolation method (respectively 07:04 vs 14:59 and 06:54 vs 14:55). Initialization time more than twice as high for the tricubic interpolation method (10 vs 4 seconds).

Table 2: results of the particle tracing tests in the Fontan dataset

	Test #	1	2	3	4	5	6	7	8	9	10	11	12
	Interpolator	QL	TC	QL	QL	QL	QL	QL	QL	QL	QL	QL	QL
	Integrator	RK45	RK45	RK23	ODE853	RK45	RK45	RK45	RK45	RK45	RK45	RK45	RK45
	Timestep [ms]	10	10	10	10	1	5	15	20	30	50	75	100
Computation time	Total [h:mm:ss]	14:53	07:03	08:07	28:51	2:25:54	29:29	10:12	07:47	05:22	04:02	04:04	03:55
	Initialization [mm:ss]	00:04	00:11	00:04	00:04	00:20	00:04	00:03	00:03	00:03	00:03	00:03	00:03
	Particle tracing [h:mm:ss]	14:50	06:53	08:03	28:47	2:25:34	29:25	10:09	07:43	05:18	03:58	04:01	03:52
	Time per particle [ms]	35	16	18	67	337	68	23	18	12	9	9	9
All particles	Seeded	25944											
	From IVC	17544 (68%)											
	From SVC	8400 (32%)											
	To LPA [%]	25.60	24.95	25.53	25.53	25.59	25.59	25.58	25.50	25.49	25.39	23.00	17.99
	To RPA [%]	53.92	53.33	53.77	54.00	53.89	53.89	53.76	53.82	52.34	46.96	39.03	31.38
	Missing [%]	19.99	20.91	20.31	20.06	20.14	20.14	19.54	18.70	17.89	16.70	15.21	12.37
	Errors [%]	0.12	0.00	0.00	0.08	0.00	0.00	0.74	1.61	3.92	10.55	22.49	38.09
IVC	To LPA [%]	37.81	36.86	37.70	37.72	37.80	37.80	37.77	37.68	37.68	37.51	33.94	26.50
	To RPA [%]	37.25	36.83	37.05	37.26	37.18	37.28	37.36	37.44	35.62	30.02	24.47	19.29
	Missing [%]	24.38	25.14	24.66	24.53	24.47	24.29	23.96	23.27	22.83	21.53	19.19	15.32
	Remaining [%]	0.53	1.17	0.59	0.47	0.55	0.63	0.55	0.54	0.53	0.60	0.42	0.25
	Errors [%]	0.02	0.00	0.00	0.02	0.00	0.00	0.35	1.07	3.34	10.34	21.99	38.64
SVC	To LPA [%]	0.11	0.06	0.11	0.08	0.08	0.11	0.12	0.06	0.04	0.06	0.14	0.20
	To RPA [%]	88.73	87.80	88.68	88.98	88.80	88.86	88.01	88.04	87.26	82.35	69.43	56.61
	Missing [%]	10.82	12.10	11.21	10.71	11.11	11.02	10.31	9.14	7.56	6.61	6.89	6.23
	Remaining [%]	0.01	0.05	0.00	0.01	0.01	0.01	0.00	0.02	0.00	0.01	0.01	0.01
	Errors [%]	0.33	0.00	0.00	0.21	0.00	0.00	1.56	2.74	5.14	10.98	23.52	36.95

IVC = Inferior Vena Cava; SVC = Superior Vena Cava; LPA = Left Pulmonary Artery; RPA = Right Pulmonary Artery; QL = Quadlinear interpolation; TC = Tricubic interpolation; RK45 = fifth order Runge-Kutta integration method; RK23 = third order Runge-Kutta integration method; ODE853 = eighth order Runge-Kutta integration method

Integration method

Tests 1, 3 and 4 had differences only in integration method. Differences in pulmonic distribution, missing particles fraction and number of integration errors are under a half percent of total particles seeded for all possible comparisons (RK45 vs RK23, RK45 vs DOP853 and RK23 vs DOP853). Total computation time and particle tracing time was almost halved for the RK23 method and almost doubled for the DOP853 method when compared to the RK45 method. Initialization time was equal for all tests, as the integration method was not part of the initialization code.

Timestep

The differences in pulmonic distribution for the tests with a timestep of 1ms to 20ms were under half a percent of total particles seeded for the particles seeded from the IVC and under one percent for particles seeded from the SVC. These differences were larger for a longer timestep, with a difference of one to two percent for a timestep of 30ms and differences of over 5 percent in most categories for longer timesteps. The missing fraction decreases with a longer timestep, whereas the number of integration errors increased greatly with a longer timestep.

The computation time and particle tracing time decreased almost proportionally with a longer timestep for timesteps up to 30ms. From 50ms on, the computation time and particle tracing time were stable at around four minutes. Initialization time was slightly lower for longer timesteps (3 vs 4 seconds). The timestep is used in the initialization code to determine how much RAM is pre-allocated to the program to save the particle traces.

Visualization

For both the interpolation method tests (test 1 and 2) and the integration method tests (test 1, 3 and 4) there were no visible differences in the visualization of the particle traces. For tests with timesteps of 20ms

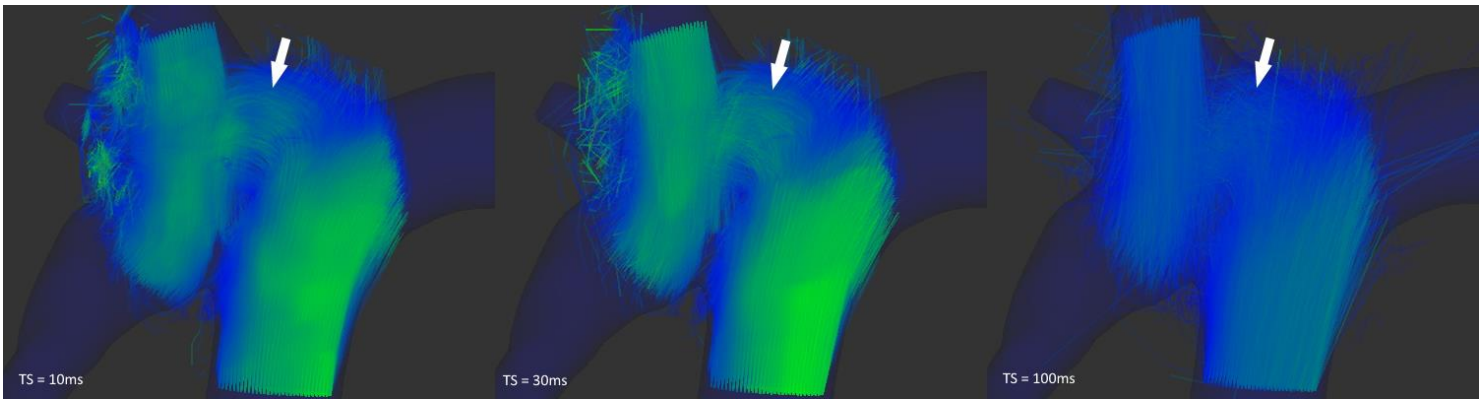

Figure 9: Visualization of pathlines in early systole for (left) test 1 with a timestep of 10ms, (middle) test 9 with a timestep of 30ms, and (right) test 12 with a timestep of 100ms. At a longer timestep, the flow patterns, e.g. the large central vortex (white arrow), become less visible and the pathlines are less smooth. Less high-speed segments of the pathlines are traced at a longer timestep. Velocity color-coding ranging from blue to green (slow to fast) was used on the pathlines. The total cavopulmonary connection segmentation model is also drawn.

and longer (test 9 to 12) there were clear differences in the visualization when compared to the visualization of test 1 with a timestep of 10ms. The main central vortex in the TCPC (white arrow in figure 9) is well recognizable with a timestep of 20ms or shorter and increasingly unrecognizable with longer timesteps. Figure 9 shows the differences in pathlines for test 1, test 9 and test 12 with a timestep of 10ms, 30ms and 100ms, respectively. The pathlines in the figure are of the early systole.

Intracardiac dataset

The results of the 12 particle tracing tests that were performed on the intracardiac dataset are noted in Table 3. Test 13 is considered the standard settings and other tests only vary in a single variable to this standard test. The interpolation method is only different for test 14, whereas the integration method varies for tests 15 and 16. The other tests, 17 to 24, have different timesteps.

Interpolation method

The four-component analysis of the quadrilinear interpolation and tricubic interpolation (test 1 and 2 respectively) only show differences of less than one percent of all particles seeded. The missing particles fraction is less than one percent of all particles seeded higher for the tricubic interpolation (10.47% vs 9.79%) and a little more than one percent higher in the four-component analysis (19.46% vs 18.37%). There was only a small difference in number of integration errors. Total computation time and particle tracing time was almost halved for the tricubic interpolation method (08:01 vs 15:15), but initialization time was about 13 seconds longer.

Table 3: results of the particle tracing tests in the intracardiac dataset

	Test #	13	14	15	16	17	18	19	20	21	22	23	24
	Interpolator	QL	TC	QL	QL	QL	QL	QL	QL	QL	QL	QL	QL
	Integrator	RK45	RK45	RK23	ODE853	RK45	RK45	RK45	RK45	RK45	RK45	RK45	RK45
	Timestep [ms]	10	10	10	10	1	5	15	20	30	50	75	100
Computation time	Total [h:mm:ss]	15:26	08:02	08:48	28:58	2:21:01	29:33	10:55	08:32	06:11	04:21	03:38	03:21
	Initialization [mm:ss]	01:05	01:18	01:05	1:05	1:06	01:05	01:05	01:06	01:05	01:06	01:05	01:05
	Particle tracing [h:mm:ss]	14:21	06:44	07:43	27:53	2:19:55	28:28	09:50	07:27	05:06	03:15	02:33	02:16
	Time per particle [ms]	046	21	25	89	446	91	31	24	16	10	8	7
All particles	Seeded	25944											
	To aorta [%]	34.45	34.65	34.37	34.34	34.17	34.07	34.82	34.67	33.20	26.86	20.30	14.31
	From left atrium [%]	43.12	42.60	43.31	43.00	43.37	43.29	43.55	43.34	42.99	41.71	39.60	34.71
	Missing [%]	18.37	19.46	18.34	18.44	18.08	18.41	18.08	18.38	18.90	17.76	16.59	13.33
	Errors [%]	0.01	0.00	0.00	0.02	0.00	0.00	0.10	0.19	1.45	8.40	19.38	32.90
4-component analysis	DF [%]	22.99	22.78	22.97	22.85	22.83	22.66	23.29	23.08	21.85	19.03	15.51	12.20
	DEF [%]	16.69	17.39	16.58	16.72	16.57	16.62	16.53	16.71	16.77	14.45	12.64	9.95
	RI [%]	23.52	23.63	23.67	23.44	23.92	23.91	23.55	23.60	24.02	25.76	27.09	26.48
	RV [%]	36.80	36.20	36.78	36.98	36.69	36.81	36.62	36.61	37.36	40.77	44.75	51.36

DF = Direct Flow; DEF = Delayed Ejection Fraction; RI = Retained Inflow; RV = Residual Volume; MP = Missing Particles; QL = Quadlinear interpolation; TC = Tricubic interpolation; RK45 = fifth order Runge-Kutta integration method; RK23 = third order Runge-Kutta integration method; ODE853 = eighth order Runge-Kutta integration method

Integration method

Differences in the four-component analysis, missing particles fraction and number of integration errors were below a half percent of all particles seeded for all possible comparisons of integration methods (RK45 vs RK23, RK45 vs DOP853 and RK23 vs DOP853). Total computation time and particle tracing time was almost doubled for the DOP853 method and almost halved for the RK23 method when compared to the RK45 method. There were no differences in initialization time.

Timestep

The differences in the missing particles fraction and the four-component analysis were below a half percent of all particles seeded for timesteps of 1ms to 20ms. From a timestep of 30ms or higher on, the particles traced to the aorta and left atrium decrease. As a result, the direct flow and delayed ejection fraction components decrease with a longer timestep and the residual volume increases. Contrarily, the retained inflow, which also depends on particles traced to the left atrium, increased as well. While the missing particles fraction decreases with a longer timestep, the number of integration errors increased greatly.

Visualizations

There are no visible differences in the visualizations of the individual particle tracing tests when varying interpolation method or integration method. There were however visible differences in the pathlines of the tests with timesteps of 20ms and longer when compared to the visualization of 10ms. With longer timesteps,

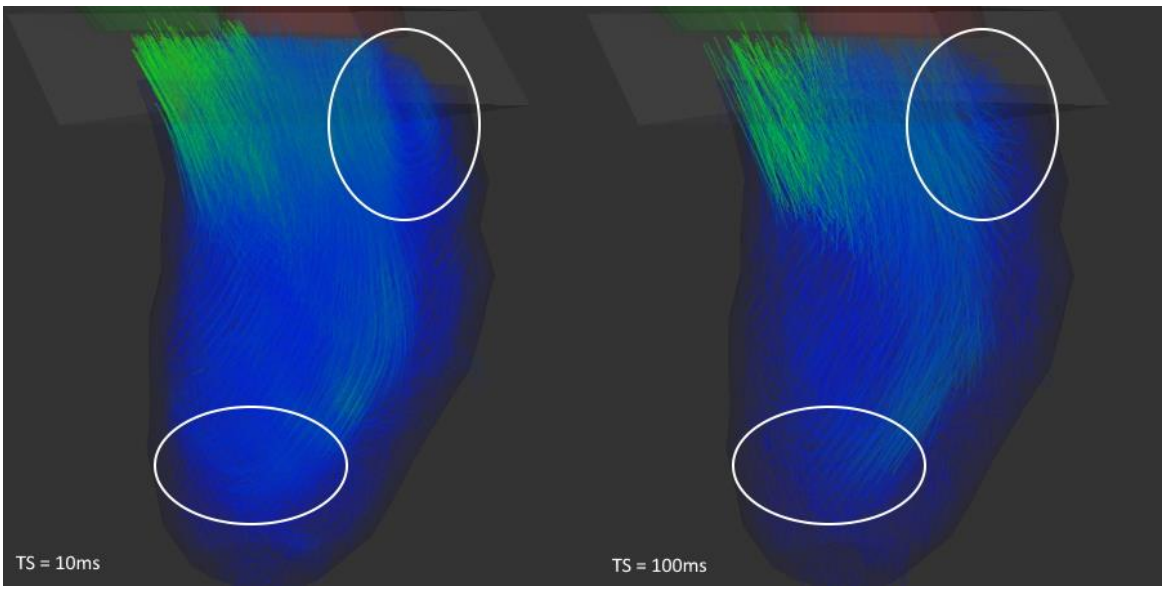

Figure 10: Visualization of pathlines in early systole for (left) test 1 with a timestep of 10ms and (right) test 12 with a timestep of 100ms. Pathlines are less smooth at a longer timestep and flow patterns (annotated by circles) such as vortices and curvatures become invisible at a longer timestep. Velocity color-coding ranging from blue to green (slow to fast) was used on the pathlines. Intracardiac segmentation models are also drawn, with green being the aortic model, red the left atrial model, dark blue the left ventricular model and colorless the connecting cuboid model.

the pathlines are less smooth and flow patterns like vortices are not visible. Figure 10 shows the differences in pathlines for test 13 and test 24 with a timestep of 10ms and 100ms, respectively. The pathlines in the figure are of the early systole.

An additional visualization was made of only the retained inflow fraction, as can be seen in figure 11. The spatial location of the particles at isovolumetric relaxation is drawn, together with the segmentation models of the aorta, left ventricle, left atrium and the connection cuboid model at the same point in. It can be seen, as depicted by the circle, that a fraction of the particles are outside of the LV segmentation model and close to the aorta segmentation model. Closer to the LV segmentation are more particles outside the model, but still within the 5mm margin and therefore still part of the retained inflow fraction.

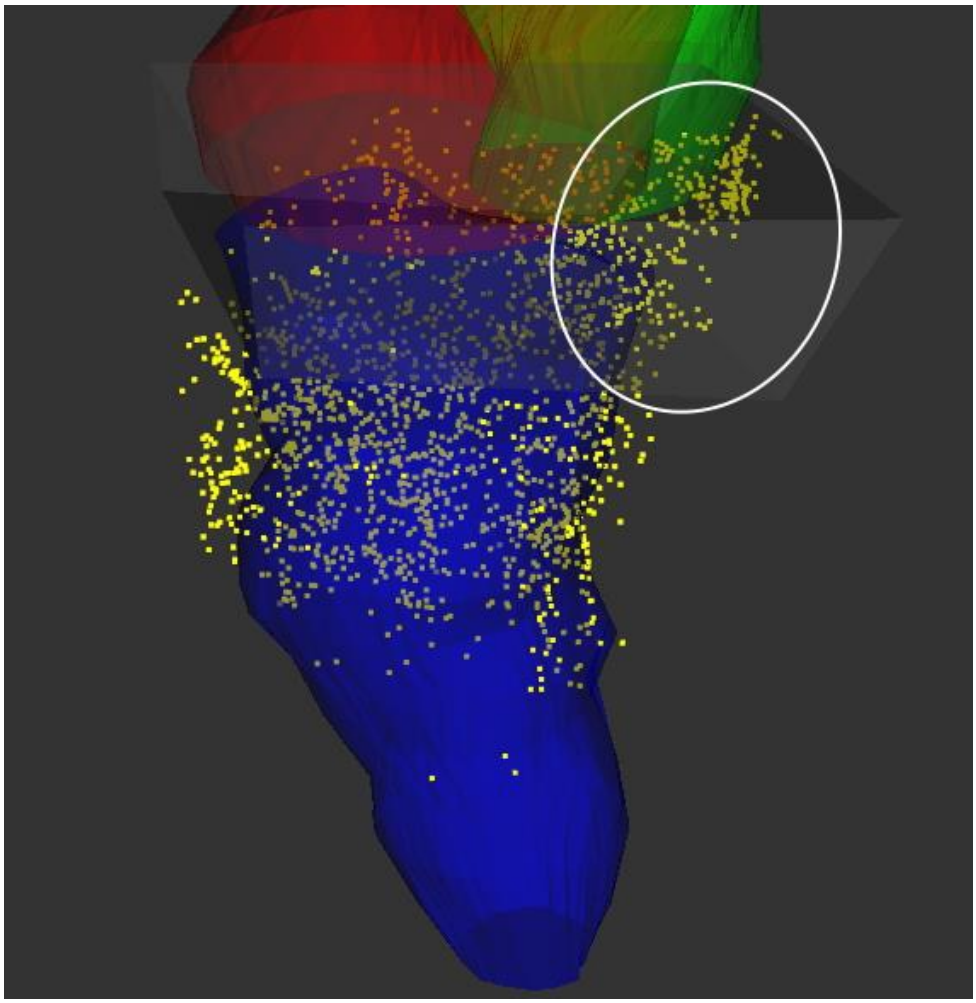

Figure 11: Visualization of the retained inflow fraction (yellow points) at isovolumetric relaxation (end-systole). Segmentation models of the left ventricle (blue), left atrium (red), aorta (green) and a cuboid (grey) connecting these structures are drawn. A fraction of the particles was outside the left ventricle model and beside the aorta model, as indicated by the white ellipse.

Discussion

In this research we have aimed to investigate the effect of integration method, timestep length and data interpolation method on the computation time and accuracy of particle tracing in 4D Flow MRI data. We have found that data interpolation method and integration method had hardly any effect on particle tracing accuracy, but they had a large effect on computation time, whereas higher order integration was more computationally expensive. The same is true for timesteps of 20ms or shorter, where a shorter timestep was more computationally expensive than a longer timestep. For timesteps of 30ms or longer, accuracy was decreased greatly.

Using the standard particle tracing settings in the Fontan dataset gave results similar to literature.[39] The missing particles fraction was around 20%, with a missing particles fraction of 24% for particles from the IVC and 11% for particles from the SVC. Although this is higher than the 20% threshold that was suggested by Ha et al., this was considered sufficient for this research.[30] The pulmonic distribution was within normal values, whereas half of the IVC particles (excluding missing and error fractions) went to either pulmonary artery (normal 55% ± 19% to LPA) and almost all SVC particles went to the RPA (normal 87% ± 13%).[39]

The standard particle tracing settings gave suboptimal results in the intracardiac dataset. Although the missing particles fraction was only around 18% and therefore under 20%, which was the threshold suggested in literature, the four-component analysis results gave a DF of 23% (normal 35% ± 6%), a DEF of 17% (normal 15% ± 3%), a RI of 24% (normal 17% ± 4%) and a RV of 37% (normal 33% ± 4%).[26,29,30,36] The DF is therefore too low and the RI too high. The DEF (here 17%) should be roughly the same as the RI (here 24%), otherwise the left ventricle would take more blood in than it would pump out, which is physiologically not realistic in a healthy heart. The DF and RI have in common that the particles reach the left atrium when tracing backwards. Further visualization of just the RI fraction showed that a portion of these particles did move in the direction of the aorta but did not enter the aortic segmentation. Instead, they moved just past the aortic model. It is possible that the segmentation of the aorta was not completely accurate and should have included this area, but further inspection of the MRI data gave no clear answer as to whether this is true.

The number of integration errors was around zero percent for both datasets with the standard settings (test 1 and 13). This did increase greatly in both datasets for tests with a timestep of 30ms or longer. It is important to note that the integration errors included errors that occurred because the data requested by the integrator was outside of the boundaries of the 4D Flow data. In longer timesteps, this can occur more often, because particles take larger temporal and spatial steps. These large steps can cause to the particle to protrude from the dataset within one step: the integrator uses data from multiple variable sub-steps (equal to the order of the integration method) to calculate the most accurate step. These particles would leave the vasculature segmentation in that step and would be considered part of the missing particles fraction. However, these errors occur within the integration step and particles are only checked if they are part of the missing fraction after the integration step. It is therefore important to note that even without the

integration error, the particles would be part of the missing fraction. Therefore, an increase in integration errors has equal importance to an increase in the missing particles fraction.

For both datasets, the choice of interpolation method did not change the missing particles fraction and PD or four-component analysis results. However, using the tricubic interpolation method did reduce the computing time by around a half. Given that tricubic spatial interpolation is traditionally more computationally expensive than trilinear spatial interpolation, this result can be explained by the method used to apply the interpolation methods. Quadrilinear interpolation was programmed in python code using simple interpolation steps to interpolate over the different dimensions sequentially. Tricubic interpolation was performed using advanced matrix multiplications, which were performed by a precompiled C++ library (Eigen3), with linear interpolation over the time dimension afterwards. The use of matrix multiplications and precompiled C++ libraries are most likely the cause for the decrease in computation time.

A higher or lower order integration method had no notable effect on the missing particles fraction and PD or four-component analysis results. It did however affect the computation time and particle tracing time: computation time was almost doubled for the eighth order integration method when compared to the commonly used fifth order integration method. The use of the third order integration method almost halved the computation time when compared to the fifth order integration method.

In both datasets, timesteps of 20ms and lower gave almost equal results in PD or four-component analysis and missing particles fraction. Timesteps of 30ms and higher gave results that can be regarded as unrealistic: up to a RV of over 50% and RI of over 30% in the intracardiac dataset for a timestep of 100ms. In the Fontan dataset, timesteps of 30ms and higher gave an increase in errors by the integrator. The integration functions gave an error for many particles because the timestep was too long to perform accurate integration or the particles left the boundaries of the flow data. Total computation time increased almost linearly proportional to the decrease of the timestep. Although the computation time in this research should not be taken as a realistic example for particle tracing in optimized clinical software, having short computation time is preferential. It is therefore advised so select a timestep as large as possible, while still maintaining adequate accuracy. A timestep of about half of the interval between cardiac phases, in this case a timestep of about 15ms, is shown to be a good starting point for performing particle tracing.

The integration functions used were part of the SciPy toolkit.[33] By origin, these integration functions were functions with an adaptive timestep: every step, a higher order integration method and a lower order integration method are used and the difference in both is seen as the error of the integration. If the error is larger than the user-defined threshold, the timestep is decreased. Otherwise, the timestep is increased until a maximum is reached. This research did not use an adaptive timestep but a fixed timestep, because the aim of this research was to investigate the effect of timestep itself on the accuracy of particle tracing. An adaptive timestep can however be useful when using particle tracing in general clinical practice.

For the Fontan dataset, a continuous seeding method was chosen. This seeding method consists of releasing particles from a (two- or three-dimensional) seeding grid at a given time interval. In this research a time interval was the same as the interval between cardiac phases and thus particles were released from the seeding grid every cardiac phase. This seeding was performed for an entire cardiac cycle to quantify blood flow throughout the entire cardiac cycle. The particles were traced until a second cardiac cycle had passed, which was long enough because of the low remaining particles fractions (less than 0.5% of all particles) in every test.

For quantification purposes of blood flow in blood vessels, such as flow distributions, it is recommended to seed throughout an entire cardiac cycle to quantify all possible flow since the cardiac cycle is a repeatable pattern and the flow within as well. It is important to trace the particles until all particles have reached a traceable destination, otherwise they will not be quantified. For visualization however, it can be beneficial to seed at only a specific time or time range within the cardiac cycle to visualize a part of the blood flow more prominently, e.g. when visualizing only systolic blood flow. Recently, Gaeta et al have described a volumetric seeding method in which particles are seeded from a grid depending on the velocity at that grid point to ensure each particle represents an equal volume of blood, which can be beneficial for quantification purposes.[21] In (temporarily) closed systems such as the heart ventricles, seeding at all voxels within the system when the blood volume is constant, e.g. at the isovolumetric contraction or relaxation, allows for quantification and visualization of all blood flow within the system when tracing both forward and backward in time. This technique could be applied on non-closed systems as well to find the origin and destination of blood volumes in certain areas. An example would be seeding particles within an aneurysm and tracing forward and backward in time to identify the blood flow within the aneurysm. This is not done in current literature today.

The segmentations of the cardiovascular structures that were used in this experiment were created by experienced physicians. For the intracardiac dataset, the segmentations were performed per slice of a short-axis scan and the individual slice segmentations were combined to a 3D model per cardiac phase. To allow room for a segmentation error, a margin of 5mm, which was approximately the length of two voxels, was defined. Further analysis into the locations where particles leave the segmentations and the MRI data itself have shown no clear inaccuracies in the segmentations. These segmentations were performed on a time-resolved short-axis scan of the heart and not on the 4D Flow MRI data itself. No registration was performed, which could be a source of error due to spatial or temporal segmentation mismatch.

The segmentation models in the intracardiac dataset were created per cardiac phase, as the size of the vasculature varied per cardiac phase. In between the cardiac phases, no interpolation of the segmentations was performed, and particles were tested if they were inside the segmentations of the temporally nearest cardiac phase. This so-called nearest-neighbor approach is in fact the simplest interpolation technique and could be replaced with a more advanced interpolation technique such as linear interpolation. Because there was no available method to perform linear shape interpolation with just the Python toolkits used in this

research, no shape interpolation was done on the segmentations. Future research might answer whether linear shape interpolation as opposed to no shape interpolation yields other or even better results for intracardiac particle tracing.

Some software packages use a user-defined minimum velocity as a stopping condition to stop tracing particles that leave the vasculature. These particles often move slowly outside of the vasculature because the flow data outside the vasculature is mostly noise, but they can move slowly if they reach flow data of another vasculature. This method of removing particles requires no segmentation and can therefore be useful for a quick visualization but is not recommended for quantification. Particles that enter areas of slow blood flow, such as aneurysms or an end-diastolic ventricle, will not be traced anymore, which could lead to inaccurate particle tracing quantifications. For this research, no minimum velocity was defined but segmentations were used to identify particles outside of the vasculature.

For the standard results, the missing particles fraction was in a normal range compared to other literature.[30,36] Physiologically however, a missing particles fraction should not exist unless the patient had a defect in the cardiovascular system, e.g. internal bleeding. No clear inaccuracies in the segmentations could be found and even with small timesteps, higher order integrations and advanced interpolation methods, no improvement in missing particles fraction could be achieved. Inaccuracies in particle tracing are therefore most likely from the data. This can be either to noise in the data or limitations in spatial or temporal resolution. It is therefore of importance to check the quality of the data before performing particle tracing. Further developments into the improvements of 4D Flow MRI data will most likely improve particle tracing as well.

Conclusion

We have performed particle tracing in two 4D Flow MRI datasets with different settings for the integration method, integration timestep and data interpolation method. Accuracy was measured quantitatively by measuring the number of particles lost during tracing, blood flow distributions and the number of integration errors, and quantitatively by visual inspection. From the results we would recommend that particle tracing is performed in 4D Flow MRI data with a low order interpolator, e.g. a third order Runge-Kutta integrator, a maximum timestep of half the temporal resolution of the data, and quadrilinear data interpolation. Besides these settings, it is important to choose a seeding method appropriate for the specific aim that particle tracing is used for. Before applying particle tracing, the quality of the 4D Flow MRI data and the segmentations of the cardiovascular structures must be inspected for artefacts and a good accuracy per cardiac phase respectively to enable a good quality of particle tracing.

Future perspectives

In this research we have explored the effect of the settings for integration method, integration timestep and data interpolation method on the accuracy of particle tracing. Several aspects of this research could be further investigated to give a broader insight into the accuracy of particle tracing. The effect of shape interpolations for the intracardiac segmentation models could be explored by comparing the results of particle tracing with and without these shape interpolations.

The segmentations were created by hand, which is time-consuming and prone to intra- and inter-operator errors. The intracardiac segmentations were not created on the 4D Flow MRI data, but on time-resolved short-axis scans. Using automatic segmentations methods on the 4D Flow MRI data directly, whether it be the magnitude data, the velocity data or both, could lead to a less time-consuming and perhaps more accurate workflow. Especially in the clinical practice this could lead to an easier adoption of particle tracing in many cardiovascular care processes. If these automatic segmentations would become more available, their effects on the accuracy of particle tracing could be studied.

4D Flow MRI is still an evolving imaging technique and further improvements could lead to better particle tracing. Both spatial and temporal resolution have effect on the particle tracing accuracy and could be improved. A limitation of these resolutions is the acquisition time, which is already reduced using advanced k-space filling techniques. Increasing acquisition speed while keeping total acquisition time the same could lead to increased spatial and temporal resolutions, and as a result possibly better particle tracing. Using multi-venc acquisition techniques can also lead to an increase in VNR and therefore could lead to better particle tracing outcomes. If new 4D Flow MRI acquisition techniques become more available, their effects on particle tracing can be studied.

References

1. Wang H, Naghavi M, Allen C, et al. Global, regional, and national life expectancy, all-cause mortality, and cause-specific mortality for 249 causes of death, 1980–2015: a systematic analysis for the Global Burden of Disease Study 2015. *Lancet*. 2016;388(10053):1459-1544. doi:10.1016/S0140-6736(16)31012-1

2. Aggarwal M, Bozkurt B, Panjrath G, et al. Lifestyle Modifications for Preventing and Treating Heart Failure. *J Am Coll Cardiol*. 2018;72(19):2391-2405. doi:10.1016/j.jacc.2018.08.2160

3. Marelli AJ, Ionescu-Ittu R, Mackie AS, Guo L, Dendukuri N, Kaouache M. Lifetime prevalence of congenital heart disease in the general population from 2000 to 2010. *Circulation*. 2014;130(9):749-756. doi:10.1161/CIRCULATIONAHA.113.008396

4. Cardiovascular disease - Acquired heart disease | Britannica. https://www.britannica.com/science/cardiovascular-disease/Risk-factors. Accessed June 22, 2020.

5. Vasan RS. Biomarkers of cardiovascular disease: Molecular basis and practical considerations. *Circulation*. 2006;113(19):2335-2362. doi:10.1161/CIRCULATIONAHA.104.482570

6. Vasan RS, Benjamin EJ. The future of cardiovascular epidemiology. *Circulation*. 2016;133(25):2626-2633. doi:10.1161/CIRCULATIONAHA.116.023528

7. Brieler J, Breeden MA, Tucker J. Cardiomyopathy: An Overview. *Am Fam Physician*. 2017;96(10):640-646.

8. Vos T, Allen C, Arora M, et al. Global, regional, and national incidence, prevalence, and years lived with disability for 310 diseases and injuries, 1990–2015: a systematic analysis for the Global Burden of Disease Study 2015. *Lancet*. 2016;388(10053):1545-1602. doi:10.1016/S0140-6736(16)31678-6

9. WHO | Global atlas on cardiovascular disease prevention and control. *WHO*. 2015. http://www.who.int/cardiovascular_diseases/publications/atlas_cvd/en/. Accessed June 22, 2020.

10. Sun RR, Liu M, Lu L, Zheng Y, Zhang P. Congenital Heart Disease: Causes, Diagnosis, Symptoms, and Treatments. *Cell Biochem Biophys*. 2015;72(3):857-860. doi:10.1007/s12013-015-0551-6

11. Stacey RB, Hundley WG. The role of cardiovascular magnetic resonance (CMR) and computed tomography (CCT) in facilitating heart failure management. *Curr Treat Options Cardiovasc Med*. 2013;15(4):373-386. doi:10.1007/s11936-013-0253-6

12. Ha H, Kim GB, Kweon J, et al. Hemodynamic measurement using four-dimensional phase-contrast MRI: Quantification of hemodynamic parameters and clinical applications. *Korean J Radiol*. 2016;17(4):445-462. doi:10.3348/kjr.2016.17.4.445

13. Kamphuis VP, Westenberg JJM, van der Palen RLF, et al. Unravelling cardiovascular disease using four dimensional flow cardiovascular magnetic resonance. *Int J Cardiovasc Imaging*. 2017;33(7):1069-1081. doi:10.1007/s10554-016-1031-9

14. Richter Y, Edelman ER. Cardiology is flow. *Circulation*. 2006;113(23):2679-2682. doi:10.1161/CIRCULATIONAHA.106.632687

15. Bernstein MA, King KF, Zhou XJ. *Handbook of MRI Pulse Sequences*. Elsevier Inc.; 2004. doi:10.1016/B978-0-12-092861-3.X5000-6

16. Stankovic Z, Allen BD, Garcia J, Jarvis KB, Markl M. 4D PC flow. *Cardiovascular*. 2014;4(2):173-

192. doi:10.3978/j.issn.2223-3652.2014.01.02

17. Sträter A, Huber A, Rudolph J, et al. 4D-Flow MRI: Technique and Applications. *RöFo - Fortschritte auf dem Gebiet der Röntgenstrahlen und der Bildgeb Verfahren*. 2018;190(11):1025-1035. doi:10.1055/a-0647-2021

18. Dyverfeldt P, Bissell M, Barker AJ, et al. 4D flow cardiovascular magnetic resonance consensus statement. *J Cardiovasc Magn Reson*. 2015;17(1):72. doi:10.1186/s12968-015-0174-5

19. Ma LE, Markl M, Chow K, Vali A, Wu C, Schnell S. Efficient triple-VENC phase-contrast MRI for improved velocity dynamic range. *Magn Reson Med*. 2020;83(2):505-520. doi:10.1002/mrm.27943

20. Markl M, Frydrychowicz A, Kozerke S, Hope M, Wieben O. 4D flow MRI. *J Magn Reson Imaging*. 2012;36(5):1015-1036. doi:10.1002/jmri.23632

21. Gaeta S, Dyverfeldt P, Eriksson J, Carlhäll CJ, Ebbers T, Bolger AF. Fixed volume particle trace emission for the analysis of left atrial blood flow using 4D Flow MRI. *Magn Reson Imaging*. 2018;47:83-88. doi:10.1016/j.mri.2017.12.008

22. Bissell MM, Dall'Armellina E, Choudhury RP. Flow vortices in the aortic root: in vivo 4D-MRI confirms predictions of Leonardo da Vinci. *Eur Heart J*. 2014;35(20):1344-1344. doi:10.1093/eurheartj/ehu011

23. Pasipoularides A. *The Heart's Vortex : Intracardiac Blood Flow Phenomena*. People's Medical Pub. House USA Ltd; 2010.

24. Anderson Jr. JD. *Computational Fluid Dynamics (CFD) in Ophthalmology*. McGraw-Hill; 1995. http://eyewiki.aao.org/Computational_Fluid_Dynamics_(CFD)_in_Ophthalmology. Accessed January 17, 2020.

25. Granger RA. *Fluid Mechanics*. Dover Publications; 1995.

26. Eriksson J, Carlhäll C, Dyverfeldt P, Engvall J, Bolger A, Ebbers T. Semi-automatic quantification of 4D left ventricular blood flow. *J Cardiovasc Magn Reson*. 2010;12(1). doi:10.1186/1532-429X-12-9

27. de Koning PJ, van der Geest RJ, Westenberg JJ. Objective method for assessment of reliability of particle tracing visualization in 4D FLOW MRI. *J Cardiovasc Magn Reson*. 2013;15(S1):E29. doi:10.1186/1532-429X-15-S1-E29

28. Van Hinsberg MAT, Boonkkamp JHMTT, Toschi F, Clercx HJH. Optimal interpolation schemes for particle tracking in turbulence. *Phys Rev E - Stat Nonlinear, Soft Matter Phys*. 2013;87(4). doi:10.1103/PhysRevE.87.043307

29. Stoll VM, Loudon M, Eriksson J, et al. Test-retest variability of left ventricular 4D flow cardiovascular magnetic resonance measurements in healthy subjects. *J Cardiovasc Magn Reson*. 2018;20(1). doi:10.1186/s12968-018-0432-4

30. Ha H, Kang H, Huh H, et al. Accuracy evaluation of blood flow distribution in the Fontan circulation: effects of resolution and velocity noise. *J Vis*. 2019;22(2):245-257. doi:10.1007/s12650-018-0536-9

31. Schroeder W, Martin K, Lorensen B. *The Visualization Toolkit*. 4th ed. Kitware; 2006.

32. Van Der Walt S, Colbert SC, Varoquaux G. The NumPy array: A structure for efficient numerical computation. *Comput Sci Eng*. 2011;13(2):22-30. doi:10.1109/MCSE.2011.37

33. Virtanen P, Gommers R, Oliphant TE, et al. SciPy 1.0: Fundamental Algorithms for ScientificComputing in Python. *Nat Methods*. 2020;17:261-272. doi:https://doi.org/10.1038/s41592-019-0686-2

34. Lekien F, Marsden J. Tricubic interpolation in three dimensions. *Int J Numer Methods Eng*. 2005;63(3):455-471. doi:10.1002/nme.1296

35. Rijnberg FM, Hazekamp MG, Wentzel JJ, et al. Energetics of blood flow in cardiovascular disease: Concept and clinical implications of adverse energetics in patients with a fontan circulation. *Circulation*. 2018;137(22):2393-2407. doi:10.1161/CIRCULATIONAHA.117.033359

36. Calkoen EE, De Koning PJH, Blom NA, et al. Disturbed intracardiac flow organization after atrioventricular septal defect correction as assessed with 4D flow magnetic resonance imaging and quantitative particle tracing. *Invest Radiol*. 2015;50(12):850-857. doi:10.1097/RLI.0000000000000194

37. Dormand JR, Prince PJ. A family of embedded Runge-Kutta formulae. *J Comput Appl Math*. 1980;6(1):19-26. doi:10.1016/0771-050X(80)90013-3

38. Hairer E, Nørsett SP, Wanner G. *Solving Ordinary Differential Equations I*. Vol 8. 1st ed. Berlin, Heidelberg: Springer Berlin Heidelberg; 1993. doi:10.1007/978-3-540-78862-1

39. Bächler P, Valverde I, Pinochet N, et al. Caval blood flow distribution in patients with Fontan circulation: Quantification by using particle traces from 4D flow MR imaging. *Radiology*. 2013;267(1):67-75. doi:10.1148/radiol.12120778

40. Krug JW, Rose G, Clifford GD, Oster J. ECG-based gating in ultra high field cardiovascular magnetic resonance using an independent component analysis approach. *J Cardiovasc Magn Reson*. 2013;15(1):104. doi:10.1186/1532-429X-15-104